Available online at www.sciencedirect.com
SCIENCE DIRECT®
Journal of Solid State Chemistry 173 (2003) 462–475
JOURNAL OF SOLID STATE CHEMISTRY
http://elsevier.com/locate/jssc

First-principles study of the structure of stoichiometric and Mn-deficient MnO_2

D. Balachandran,[a] D. Morgan,[a,*] G. Ceder,[a] and A. van de Walle[b]

[a] *Department of Materials Science and Engineering, Massachusetts Institute of Technology, Cambridge, MA 02139, USA*
[b] *Department of Materials Science and Engineering, Northwestern University, Evanston, IL 60208, USA*

Received 27 September 2002; received in revised form 15 November 2002; accepted 9 December 2002

Abstract

We present an extensive Density Functional Theory study on the phases and magnetic states of MnO_2, with over 300 calculations of various Mn–vacancy configurations and magnetic spin states. It is shown that the paramagnetic extrapolations of spin-polarized results are essential to correctly reproduce pyrolusite as the ground state of MnO_2. Paramagnetic energies are obtained by fitting a Heisenberg Hamiltonian to the energy of 10–20 magnetic configurations for each of 16 possible MnO_2 polymorphs. Near groundstate degeneracy is shown to occur due to the frustration of otherwise large interactions. While many other structures are found to be near degenerate in energy with pyrolusite, no thermal disorder exists in the system up to several thousand degrees. The thermal disorder is suppressed because the strong correlation of the Mn–vacancy order along the lines of face-sharing octahedra removes any low-energy excitations from the system. Mn vacancies compensated by protons (Ruetschi defects), ubiquitously present in commercial MnO_2, are shown to have a dramatic effect on phase stability. The stabilizing effects of Ruetschi defects may explain the presence in MnO_2 of ramsdellite and twinning, both of which are unstable in the pure material. We believe Ruetschi defects to be an important source of the structural complexity of synthetic MnO_2 produced either electrochemically or chemically.

1. Introduction

The alkaline Zn/MnO_2 system has become the dominant chemistry used for primary batteries. About 200,000 metric tons of manganese dioxide is used annually as cathode material in alkaline cells [1], and significant effort is expended in a continual attempt to optimize and improve the material.

Natural and synthetic manganese dioxide can be found in a large number of different forms. The electrochemically active form of MnO_2 presently used in alkaline batteries is commonly referred to as γ-MnO_2. Based on the method of production, γ-MnO_2 can be categorized into natural manganese dioxides (NMDs), chemical manganese dioxides (CMDs), and electrolytic manganese dioxides (EMDs). The γ-MnO_2 polymorph does not denote a unique structure but has been suggested to be either a single phase with considerable disorder [2] or a multi-phase assembly [3]. All of the relevant phases of MnO_2 in this study consist of a (possibly distorted) hexagonal close packed (hcp) lattice of oxygen ions with Mn cations occupying half the octahedral sites.

A number of different names have been given to specific arrangements of the Mn atoms in such a close-packed oxygen framework, of which pyrolusite (β-MnO_2) is generally regarded as the most stable structure (see Figs. 1 and 2) [2].

In addition to pyrolusite, γ-MnO_2 has been claimed to contain ramsdellite (R-MnO_2), ε-MnO_2, and other polymorphs. Ramsdellite, perhaps with extensive defects, is often thought to be the dominant structure in γ-MnO_2, and it is also shown in Figs. 1 and 2. Highly textured fibrous samples of manganese dioxide that are prepared electrochemically are designated as ε-MnO_2. This structure has been described by De Wolf et al. [4] as a hexagonal closed packing of O^{2-} with Mn^{4+} stochastically distributed over half the available octahedral interstices (similar to the NiAs structure), though more recently, ordered versions of ε-MnO_2 have also been proposed [3].

The γ-MnO_2 polymorph is a highly disordered material. After a thorough analysis of X-ray data,

*Corresponding author. Fax: +1-617-258-6534.
E-mail address: dmorgan@mit.edu (D. Morgan).

0022-4596/03/$ - see front matter © 2003 Elsevier Science (USA). All rights reserved.
doi:10.1016/S0022-4596(03)00023-9

Chabre and Pannetier [2] proposed that γ-MnO_2 be thought of as consisting of varying amounts of De Wolff disorder [5] (intergrowth of pyrolusite and ramsdellite units) and microtwinning (pictured in Fig. 3). Although this approach to understanding γ-MnO_2 is applied widely, many other perspectives exist.

Simon et al. [6] developed a Rietveld refinement model to explain the characteristics of the XRD patterns for a wide variety of EMD samples. In contrast to Chabre and Pannetier, who disregard ε-MnO_2 as a component of EMD, Simon et al. incorporate it as one of the possible phases in the Rietveld model. Their model describes EMD as a binary mixture of ε-MnO_2 and pyrolusite–ramsdellite intergrowth (which they call

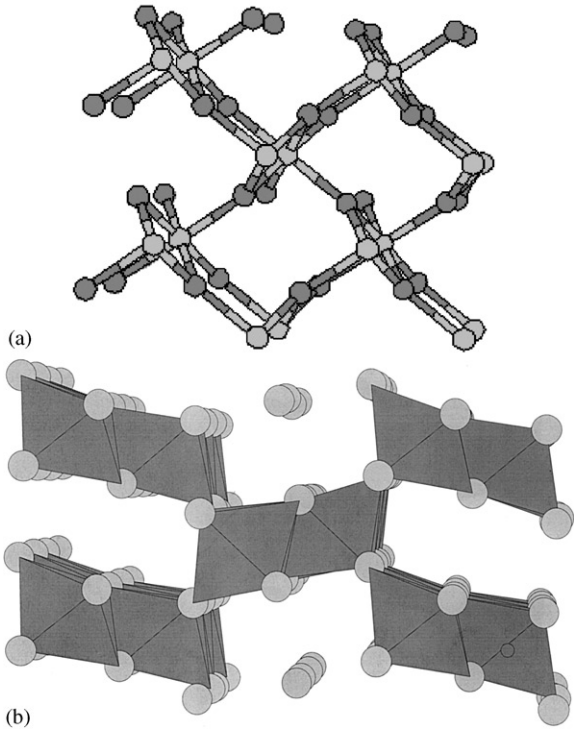

Fig. 1. Schematic representation of the structure of (a) pyrolusite and (b) ramsdellite. Oxygen are light gray circles. Mn Octahedra are dark gray.

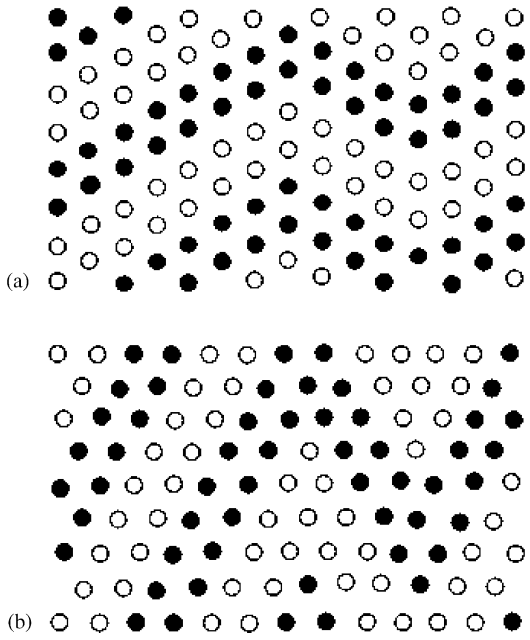

Fig. 3. Microtwinning of an ideal ramsdellite lattice on (a) [061] plane and (b) [021] plane (filled circles: Mn^{4+} at $z = 1/2$; open circles: Mn^{4+} at $z = 0$). Coordinate z is along the c-axis, perpendicular to the basal plane and the page.

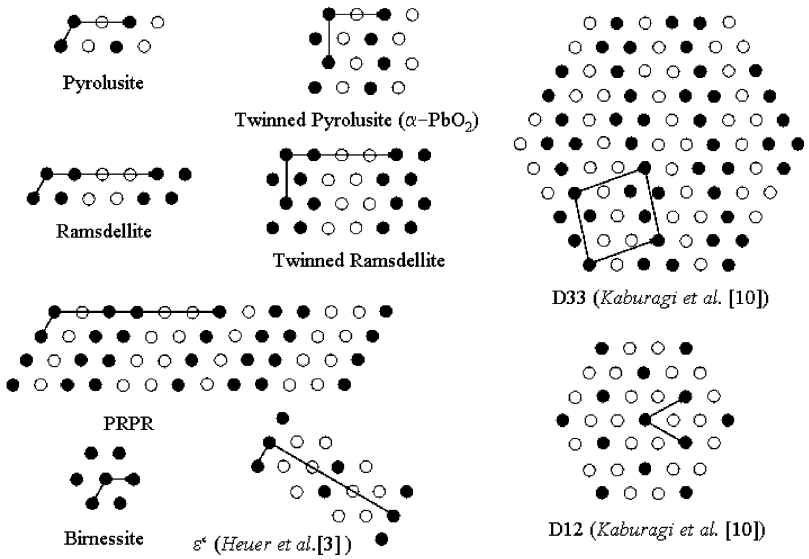

Fig. 2. Schematic pictures of unit cells for important polymorphs of MnO_2. Filled and empty circles denote Mn and vacancies, respectively. Oxygen are not shown. Only one basal plane is shown, but the adjacent basal planes can be found by interchanging Mn atoms and vacancies.

γ-MnO_2) crystallites with different crystallite domain sizes. Following Chabre and Pannetier, their model incorporates microtwinning and De Wolff disorder in the intergrowth phase.

The microstructure and crystallography of EMD was studied by Heuer et al. [3] using transmission electron microscopy (TEM). Based on the TEM data, they described EMD as a heterogeneous phase system, partially consistent with Simon's results. They found that the overall material contains $\sim$50% ramsdellite, $\sim$30% ε-MnO_2, and $\sim$15% pyrolusite. They also believe that Mn–vacancy ordering is present in ε-MnO_2 (in accordance with De Wolf et al. [4]) and suggest a model for a fully ordered form of ε-MnO_2, which they call ε'-MnO_2 (shown in Fig. 2). However, no evidence for microtwinning was found in their EMD samples.

Bowden et al. [7] provided an alternative interpretation of the γ-MnO_2 structure. They performed convergent beam electron diffraction (CBED) experiments on EMD powder. The CBED patterns revealed streaks of intensity in the reciprocal space, which they interpret to be resulting from two-dimensional (2D) sheets of scattered intensity perpendicular to the c-axis ([001] direction). Traditionally, sheets of intensity in reciprocal space have been interpreted in terms of *linear disorder* [8]. This disorder involves an absence of periodicity in all but one direction (the c-axis). The results of Bowden et al. are consistent with those of Chabre and Pannetier, since the combination of De Wolff defects and extensive twin defects produces the *linear disorder* that results in the observed sheets of intensity in reciprocal space. Bowden et al. indicate that EMD consists of randomly oriented homogeneous ramsdellite crystallites distorted by the presence of 1D pyrolusite defects and extensive twin defects.

In the present work, we demonstrate the use of computational methods to investigate the polymorphs of γ-MnO_2 and try to understand the reasons for its structural complexity. In Section 2, we describe the methodology used to perform the computations. Throughout this work, Density Functional Theory with ab initio pseudopotentials was used to compute the total energies of various structures. Using the energetics of a small number of compounds, the energy of the solid is parameterized with a lattice model for the Mn–vacancy arrangement, enabling us to calculate the energy of any arrangement of atoms within the lattice at a given composition. Finally, the energy model is used in conjunction with statistical mechanical methods to determine thermodynamic properties for the system. In Section 3, the energetics of different Mn arrangements are reviewed. We identify the dominant interactions and introduce the low-energy structures for MnO_2. Section 4 deals with the thermodynamic properties of the system, including the ground state, nature of excitations, and the transition temperature for Mn–vacancy disorder. The effects of defects on the structural stability of γ-MnO_2 are investigated in Section 5.

2. Methodology

2.1. Lattice models

As mentioned earlier, γ-MnO_2 can be thought of as consisting of an hcp oxygen framework, with Mn and vacancies each occupying half of the hcp lattice's octahedral sites. The hcp octahedral sites form a simple hexagonal lattice and all the MnO_2 polymorphs relevant to γ-MnO_2 can be understood as different Mn–vacancy arrangements on this hexagonal lattice. There are many other MnO_2 polymorphs (e.g., those based on a face centered cubic lattice of oxygen) but these do not seem to appear as a substantial phase fraction in γ-MnO_2 materials. Hence, the problem of understanding MnO_2 structures can be formally approached by investigating the ordered states of a binary alloy (Mn and vacancies are the constituents) on a simple hexagonal lattice.

2.1.1. The 2D picture

A common feature to almost all of the important MnO_2 structures is that Mn atoms never simultaneously occupy two sites in adjacent hexagonal planes that differ only by a displacement along the c-axis. These sites are quite close together and the large electrostatic repulsion between Mn^{4+} prevents their simultaneous occupation. Because of this constraint, knowledge of the Mn arrangement in a single hexagonal plane immediately tells us the occupations of all the other planes. Therefore, the problem of characterizing the Mn–vacancy configuration can be reduced to considering only a single hexagonal plane.

2D lattice models can be quite useful for understanding the possible Mn–vacancy arrangements on a simple hexagonal plane. Chabre and Pannetier [2] have constructed a ground state map showing the region of stability for several of the known MnO_2 polymorphs as function of the strength of the effective Mn–vacancy interactions. Only the first three pair interactions between Mn sites were assumed to be non-zero in this model. Earlier, Kaburagi and Kanamori [9] computed a more complete ground state map for the first three pair interactions on a hexagonal lattice. This map, shown in Fig. 4, displays all the structures with half the octahedral sites occupied by Mn that can be stable when varying the interactions. Even though Fig. 4 identifies many of the commonly seen MnO_2 structures, it does not explain the *simultaneous* presence of these phases in γ-MnO_2. In fact, since the structures on a ground state map are mutually exclusive in equilibrium, the ground state map actually suggests that the different phases should *not* be

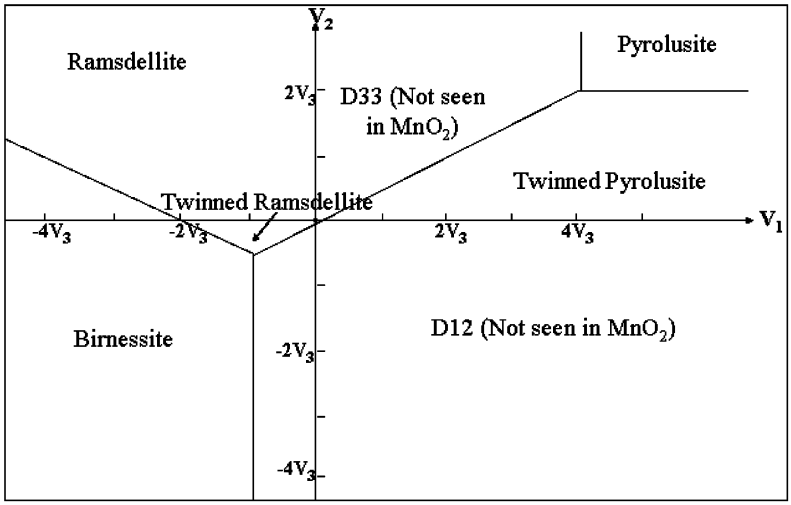

Fig. 4. The ground state map for the first three nearest-neighbor interactions on a hexagonal plane (adapted from [9]). The map corresponds to $V_3<0$. The notation D12 and D33 is taken from [9].

simultaneously present in γ-MnO_2. Pictures for each of the different structures in the ground state map as well as a few others, represented by the occupations of a single hexagonal plane, are shown in Fig. 2.

2.2. Cluster expansion

To study defects and thermal disorder in MnO_2, the energy of many Mn–vacancy arrangements may need to be evaluated. These evaluations can be done conveniently using lattice models for the energy of various Mn–vacancy arrangements. The application of lattice models to the thermodynamics of partially disordered systems such as MnO_2 can be well justified and extended to arbitrary sets of interactions. In alloy theory [10] it has been shown that in systems with configurational (ionic disorder), a lattice model formalism arises naturally when coarse-graining the partition function of the system over faster degrees of freedom. To characterize a given Mn configuration for a structure, it is useful to introduce occupation variables σ_i for each lattice site i, which is $+1$ if a Mn ion occupies site i and -1 if site i is vacant. If we now let $\{\sigma\}$ represent a specific set of octahedral interstices that are occupied, and $\{\tau\}$ represents the state of all other degrees of freedom (e.g. positional, electronic, or magnetic), the partition function of the material can be written as

$$Z=\sum_{\{\sigma\}}\sum_{\{\tau\{\sigma\}\}}\exp\left(\frac{-E(\{\sigma\},\{\tau\{\sigma\}\})}{kT}\right). \quad (1)$$

The first summation contains all the different possible distributions of Mn over the octahedral sites. The second summation is over the faster excitations that can exist in a given configuration $\{\sigma\}$. This ensemble of excitations is labeled as $\tau\{\sigma\}$. The effect of the fast excitations can be reduced to an *effective* configurational Hamiltonian, $F(\{\sigma\})$, for the $\{\sigma\}$ degrees of freedom, by formally replacing the inner sum

$$F(\{\sigma\})=-kT\ln\left[\sum_{(\text{fast}\{\sigma\})}\exp\left(\frac{-E(\{\sigma\},\{\text{fast}\{\sigma\}\})}{kT}\right)\right]. \quad (2)$$

This allows the partition function of the system to be written as

$$Z=\sum_{\{\sigma\}}\exp\left(\frac{-F(\{\sigma\})}{kT}\right). \quad (3)$$

Eq. (3) is the partition function of a lattice model. Applying lattice model statistical mechanics to $F(\{\sigma\})$ will therefore give the thermodynamic properties of the true system. Eq. (2) can be seen as one step toward systematically removing degrees of freedom from a system. $F(\{\sigma\})$ incorporates the effect of all vibrational, electronic, magnetic, etc. disorder and can be thought of as a *free energy* for these excitations in an ensemble of fixed configuration $\{\sigma\}$. In the last step (Eq. (3)), the effect of configurational disorder is then added. In many cases $F(\{\sigma\})$ can be approximated by the lowest energy term in the ensemble $\tau(\{\sigma\})$. This means the lowest energy state $E^0\{\sigma\}$ for a fixed configuration $\{\sigma\}$. Practically, this state is found by placing the Mn ions in configuration $\{\sigma\}$ on the ideal octahedral lattice and relaxing the system until the lowest energy is obtained. Such an approach amounts to neglecting all other entropy effects besides configurational entropy and is widely used in the first-principles calculation of phase diagrams. In this work, we will go beyond this approach and include the effect of magnetic excitations in the lattice model Hamiltonian (Eq. (2)). For the important

low-energy Mn distributions in the octahedral sites we will integrate over the disorder of the magnetic spins on the Mn^{4+} ions, since these materials are paramagnetic at room temperature and magnetism has been found to play an essential role in stabilizing the correct ground states in manganese oxides [11]. Vibrational entropy will not be included, though it could be incorporated with recently proposed methods [12].

The description in terms of configurational variables $\{\sigma\}$ needs to be distinguished from one in terms of real positions of ions. The state $\{\sigma\}$ is only a label to describe which ion is associated with which lattice site (i.e. which octahedral interstice). It does not assume that the ions sit exactly at the sites of some "ideal" lattice. Rather, the label $\{\sigma\}$ represents the relaxed state of the ions in that configuration.

For a system with N sites that can be occupied by two species there are 2^N possible configurations. It is therefore impossible to calculate $F\{\sigma\}$ for each possible configuration for realistic values of N. The solution to this problem is to construct a rapidly converging expansion for $F\{\sigma\}$ in terms of a set of variables that describe the configurational state. Such a set of variables is given by the *cluster functions* [13]. For a collection of lattice sites (the cluster α), the cluster function ϕ_α is defined as the product of all occupation variables in that cluster:

$$\phi_\alpha = \prod_{i\in\alpha} \sigma_i. \tag{4}$$

If a cluster function for each possible cluster of sites on the lattice is included, this basis set of functions is complete [13], so any property of configuration can be written in this basis up to arbitrary accuracy. Such an expansion is referred to as a *cluster expansion* (CE). This is somewhat of a misnomer as the clusters α are not clusters of atoms in a physical sense. They merely represent clusters of configurational variables in an infinite system. A more appropriate term would be to call it a *configurational* expansion. The thermal and spatial average of a cluster function (averaged over all the clusters that are equivalent by symmetry) is called a *correlation function*. For example, a state in which all Mn ions have vacancies in the nearest-neighbor position would always have the nearest-neighbor cluster functions equal to $(+1)\cdot(-1) = -1$, and the correlation function would be -1. Correlation functions for common structures of MnO_2 are given in Table 1, and give a powerful way to numerically represent a structure.

The energy can be expanded in cluster functions:

$$F(\{\sigma\}) = \sum_\alpha V_\alpha \phi_\alpha(\{\sigma\}). \tag{5}$$

The expansion coefficients, V_α, are referred to as effective cluster interactions (ECIs). Practically, they are obtained by calculating the energy of a series of configurations $\{\sigma\}$ and then fitting a truncated form of Eq. (5) to the values of E^0 obtained. In this work, we use the cross-validation method to optimize the quality of the fit [14]. The CE approach has been used previously on many similar problems, e.g., to analyze Li–vacancy disorder in Li_xCoO_2 [15].

The energies of all configurations in this work are computed in the generalized gradient approximation (GGA) to Density Functional Theory. The wave functions are expanded in plane waves up to a cutoff energy of 405 eV and the cores are represented with ultra-soft pseudopotentials, as implemented in the Vienna Ab Initio Simulation Package (VASP) [16,17]. Calculations were converged to within a few meV per MnO_2 formula unit with respect to k-point sampling in the Brillouin zone and the number of plane-wave basis functions (for the primitive unit cell of six atoms, we used a $5\times5\times5$ Monkhorst-Pack mesh centered at Γ). The energies of a large number of Mn configurations (36) were calculated with ferromagnetic spin polarization. For about 16 of the most important structures, a number of antiferromagnetic arrangements were also computed. By fitting these to a Heisenberg model, the paramagnetic energy could be estimated [18].

3. Energy of MnO_2 configurations and CE

3.1. Ferromagnetic and paramagnetic energies

Table 1 shows the energy as computed with GGA for a large number of MnO_2 arrangements. In each case, the energy is per formula unit and referenced to that of the paramagnetic pyrolusite. The well-known arrangements are numbered and listed by name, whereas the other structures are only numbered, but can be identified from the correlations. Pictures of all the structures mentioned in the following paragraph can be found in Fig. 2. The ε' structure is the one recently proposed by Heuer et al. [3] in EMD. Arrangements denoted by α-PbO_2 and Tw-R represent fully twinned pyrolusite and fully twinned ramsdellite, respectively [2]. PRPR consists of alternate ramsdellite and pyrolusite building blocks. The D33 structure is a possible ground state of the 2D hexagonal lattice that was identified in the ground state study of Kaburagi and Kanamori [9] as lying between pyrolusite and ramsdellite in interaction space. Birnessite is the mineral in which manganese fully occupies alternating layers of octahedral sites perpendicular to the c-axis of the hcp oxygen stacking. From the calculated energies one can see that these structures make up most of the low-energy arrangements, thereby giving an indication of why they may be most common in nature. Most other arrangements that were made by us (numbered from 11 to 38 in Table 1) have higher energy. Magnetism plays a

Table 1
Pair correlations and energies for 38 MnO_2 polymorphs

Name	Ferro energy (meV/FU)	Para energy (meV/FU)	1NN	2NN	3NN	4NN	5NN	6NN
1 Pyrolusite	67	0	−1.00	−0.33	0.33	1.00	−0.33	0.33
2 (e′)	58	16	−1.00	0.11	−0.11	1.00	−0.33	0.33
3 (Rams)	64	22	−1.00	0.33	−0.33	1.00	−0.33	0.33
4 (a-PbO_2)	80	37	−1.00	−0.33	0.33	1.00	0.33	−0.33
5 (D33)	85	40	−1.00	0.00	0.00	1.00	−0.33	0.33
6 (PRPR)	62		−1.00	0.11	−0.11	1.00	−0.33	0.33
7	92	79	−1.00	0.33	−0.33	1.00	0.00	0.00
8 (Tw-R)	114		−1.00	0.33	−0.33	1.00	0.00	0.00
9	233	157	−1.00	−0.33	0.33	1.00	1.00	−1.00
10 (Birn)	163	162	−1.00	1.00	−1.00	1.00	1.00	−1.00
11	238	201	−1.00	0.00	0.00	1.00	0.00	0.00
12	225		−1.00	0.00	0.00	1.00	0.33	−0.33
13	271	252	−0.33	−0.33	0.00	−0.33	1.00	−0.33
14	364		−0.56	−0.11	−0.04	0.56	−0.33	0.33
15	368		−0.50	0.00	−0.17	0.00	0.33	−0.17
16	405		−0.50	0.00	−0.17	0.00	0.00	−0.17
17	421	407	0.33	−0.33	−0.33	−0.33	1.00	0.33
18	438		0.00	0.00	−0.33	1.00	0.33	−0.33
19	440		0.00	0.00	−0.33	1.00	0.33	0.00
20	556		−0.50	0.33	−0.33	0.00	0.00	−0.17
21	608		0.00	−0.33	0.00	0.00	0.00	0.00
22	661	663	0.00	−0.33	0.00	−1.00	−0.33	0.00
23	669		0.00	0.00	−0.33	0.00	0.00	−0.33
24	711		0.33	0.11	−0.11	−0.33	−0.33	−0.33
25	748		−0.50	0.33	−0.17	0.00	−0.33	0.17
26	782	763	−0.33	0.11	−0.11	−0.33	−0.33	0.00
27	764		0.00	0.00	0.00	−0.50	−0.33	0.00
28	859	826	0.33	−0.33	−0.33	1.00	1.00	0.33
29	1075		0.00	0.00	0.00	1.00	−0.33	0.00
30	1096		0.00	0.33	−0.33	1.00	0.00	−0.33
31	1205		0.00	0.33	−0.17	0.00	0.00	−0.33
32	1303	1286	0.33	0.11	−0.11	1.00	−0.33	−0.33
33	1294		0.00	0.33	0.00	1.00	−0.33	0.00
34	1299		0.00	0.33	0.00	1.00	0.00	−0.33
35	1454		−0.50	1.00	−0.50	0.00	1.00	−0.50
36	1454		−0.50	1.00	−0.50	0.00	1.00	−0.50
37	1479		0.50	0.33	0.17	0.00	−0.33	−0.17
38	1548	1551	1.00	−0.33	−0.33	1.00	−0.33	−0.33

Structures are ordered according to their energy (the ordering uses paramagnetic energies when available, otherwise ferromagnetic energies are used). The key structures are named - "Rams," "Tw-R," and "Birn" refer to ramsdellite, twinned ramsdellite, and birnessite, respectively. All the named structures are shown in Fig. 2. All energies are relative to the energy of paramagnetic pyrolusite. The second and third columns list the energy obtained for ferromagnetic and paramagnetic Mn spin arrangements, respectively.

key role in the relative stability of the low-lying structures. For a ferromagnetic spin arrangement, the ε' structure is actually the ground state among all the structures that we considered, which does not seem to agree with the experimental observation that pyrolusite is the most stable form of MnO_2. Pyrolusite is recovered as the ground state in the paramagnetic computation. The MnO_2 systems are antiferromagnetic at low temperature [19] and paramagnetic at room temperature. The energy of a paramagnetic spin configuration cannot be directly obtained from the first-principles methods used in this work. Hence, in order to obtain the paramagnetic energy of a structure, the energy of the structure is calculated with various magnetic arrangements (about 20 per structure), and these energies (relative to ferromagnetic energy) are then fit to a Heisenberg Hamiltonian. The constant term of this fit gives the difference between the paramagnetic and ferromagnetic energies of the particular Mn–vacancy arrangement (ΔE). An example of this magnetic CE fit is shown in Table 2, which gives values for the magnetic interactions in a few MnO_2 polymorphs. The table shows that magnetic interaction can vary significantly, depending upon the Mn–vacancy configuration.

These results therefore stress the importance of properly treating the magnetic state when performing computations on Mn oxides [11]. Very often spin-polarized computations are reported with ferromagnetic

Table 2
Magnetic cluster expansion fits for various MnO_2 polymorphs

Clusters	Birnessite	ε'-MnO_2	Rams	Pyro
Constant (ΔE)	2	−42	−42	−67
1NN	NA	NA	NA	NA
2NN	−5	3	4	15
3NN	NA	13	19	10
4NN	0	3	3	3
5NN	0	3	0	NA

The constant term in the fit indicates the difference between paramagnetic and ferromagnetic energies (ΔE) for the structure. The neighbor shells are indexed on the simple hexagonal Mn–vacancy sublattice of octahedral sites. Specific Mn–vacancy arrangements may have no Mn–Mn pairs for a given neighbor shell and therefore have no magnetic interaction for that neighbor. These cases are entered as not applicable (NA) in the table. All interactions are in meV.

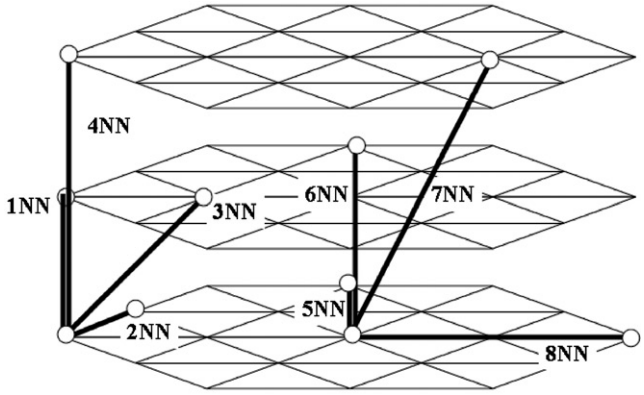

Fig. 5. Illustration of the 1st–8th nearest-neighbor pairs on a hexagonal lattice.

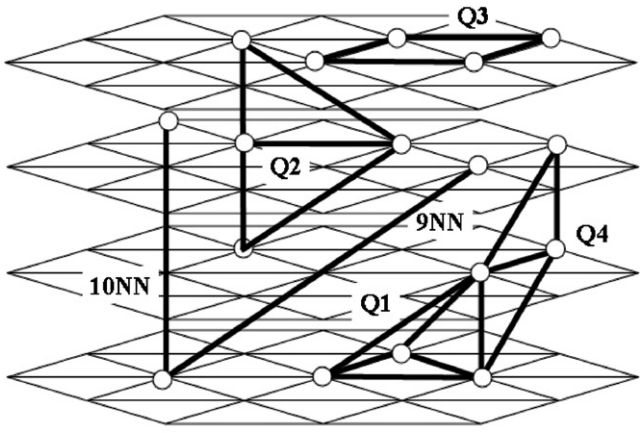

Fig. 6. Illustration of 9th and 10th nearest-neighbor pairs and select quadruplets on a hexagonal lattice.

spins, as this leads to a unit cell that is the same as the one determined by the ions. Clearly, as in the case of Mn^{3+} ions [11], this can give incorrect results for the relative stability of the different Mn arrangements.

Note that the ε' structure, proposed by Heuer et al. [3] based on XRD and TEM diffraction, is also very low in energy. This structure is a fully vacancy ordered version of ε-MnO_2, in which the hcp oxygen sublattice of NiAs is maintained but in which certain cation sites in NiAs are either fully occupied by Mn^{4+} cations or are vacant.

Several of the MnO_2 structures have very similar energy, often differing by less than the thermal energy at room temperature. Therefore, significant thermal disorder in a real MnO_2 material might be expected, even at low temperatures. In Section 4 we show that this argument needs to be made more carefully and that while *defect-induced* disorder may exist, pyrolusite has no *equilibrium* thermal disorder at temperatures below $\approx$4,000 K.

3.2. CE of Mn–vacancy disorder

Only for a limited number of MnO_2 configurations can one calculate the total energy directly with Density Functional Theory. The energies in Table 1 can be used to parameterize a CE which in turn gives the energy of any Mn–vacancy configuration and can be used in non-zero temperature simulations.

CE involves fitting the ECIs in Eq. (5) with the energies of known structures. As it is easier to calculate the energy of ferromagnetic MnO_2, the CE was performed with these ferromagnetic energies. A "paramagnetic correction" to the ECI was then determined by cluster expanding the difference between the ferromagnetic and paramagnetic energies were available. The various clusters involved in this calculation are shown in Figs. 5 and 6. In addition to a constant, 10 pair clusters and four quadruplet clusters were used for the ferromagnetic fit. Since MnO_2 has 50% Mn atoms and 50% vacancies, all the three-point correlations are generally zero and hence no triplet terms were included in the fit. Similarly, the point ECI was set to zero. For the ferromagnetic fit, 38 structural energies were used to fit 15 ECIs. The cross-validation method was also used to optimize the quality of the fit [14]. Note that all interactions and energies are normalized to one formula unit. Paramagnetic correction ECI were fitted to the difference between the ferromagnetic and paramagnetic energy for 16 structures (with typically 20 magnetic configurations used for each structure). Because the input is limited to 16 structures, only the first four pair clusters in the Mn–vacancy CE were used for the paramagnetic-correction fit. With the two sets of interactions the paramagnetic energies for all the 38 structures in Table 1 could be calculated. These total paramagnetic energies were then fit to yield a set of total ECI. The strengths of these total interactions describing the paramagnetic energy are shown in Fig. 7. Table 3 gives the values for the ferromagnetic, paramagnetic-correction, and total paramagnetic energy cluster

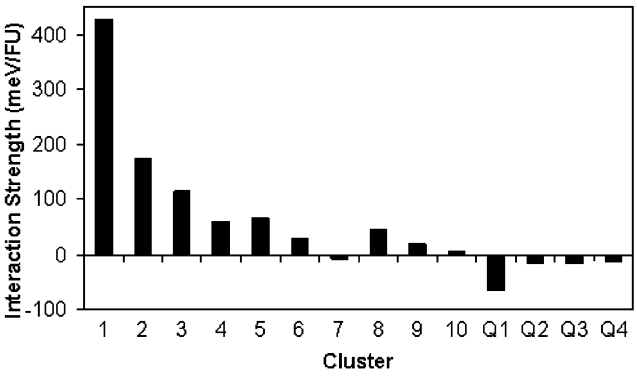

Fig. 7. ECI for MnO_2 based on total paramagnetic energies.

Table 3
Values for the ferromagnetic, paramagnetic correction, and total paramagnetic ECIs in MnO_2

Cluster	Multiplicity	Ferro ECI	Para correction	Total ECI
Const.	1	−23060	2	−23073
1NN	2	435	13	439
2NN	6	196	9	178
3NN	12	134	1	141
4NN	2	72	−10	87
5NN	6	84	—	67
6NN	12	42	—	31
7NN	12	−6	—	4
8NN	6	59	—	56
9NN	12	27	—	23
10NN	6	7	—	3
Q1	6	−64	—	−68
Q2	2	−18	—	−13
Q3	12	−17	—	−16
Q4	6	−12	—	−19

The multiplicity for each cluster is also shown in the table. All interactions are in meV.

interactions. Note that our fitting methods uses a weighted least squares minimization. Since the weighting is different for the different fits, the total ECI are not the sum of the ferromagnetic and paramagnetic-correction ECI.

3.3. Discussion of energetics

The close energy of many of the structures seems at odds with the large values for the ECI. The first three ECI in Fig. 7 are all above 100 meV, with the nearest-neighbor ECI being more than 400 meV. Part of the close energy competition between various structures arises because of the geometric frustration between these first three interactions (see Fig. 8). V_1 points between an octahedral site and the octahedral site directly above it (in the direction of the c-axis). V_2 is the nearest neighbor in the hexagonal plane of octahedral sites perpendicular to the c-axis and the vector defining V_3 is the sum of the vectors of V_1 and V_2. Together these three interactions

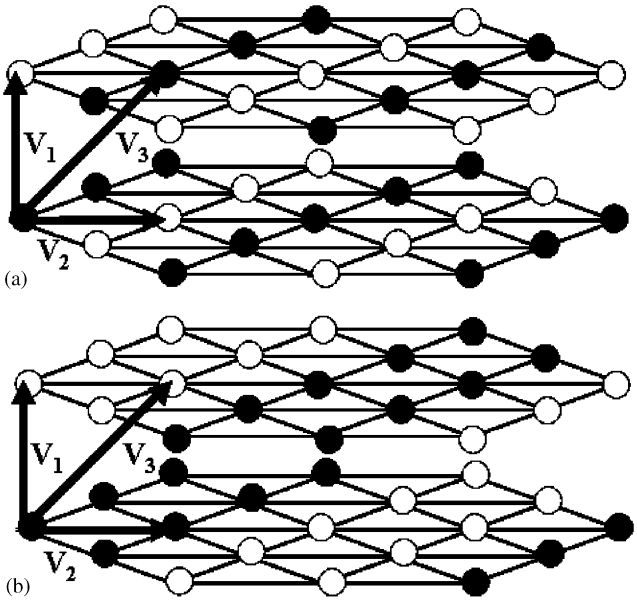

Fig. 8. Frustration in pyrolusite (a) and ramsdellite (b). The first three nearest-neighbor interactions are shown in the figure. Filled and empty circles represent Mn and vacancies, respectively.

form a triangle along which only repulsive interactions exist. Since it is not possible to organize Mn and vacancies on the vertices of a triangle so that all edges are Mn–vacancy edges, the system is frustrated. This implies that at least one of the first three pair interactions is always "unsatisfied", i.e. it has a Mn–Mn bond, which gives a high energy due to the repulsive interaction. It is in part this frustration which leads to the large number of structures with close energies. Pyrolusite and ramsdellite can be seen as two different answers to this frustration (Figs. 8 (a) and (b), respectively). In pyrolusite, more in-plane nearest-neighbor bonds (V_2) are Mn–vacancy, but less V_3 interactions are satisfied than in ramsdellite. This can be seen from the correlations for these two structures in Table 1. The second-neighbor correlation for pyrolusite is $-\frac{1}{3}$, implying that it has more unlike nearest-neighbor bonds in the plane than ramsdellite, with a correlation of $+\frac{1}{3}$. The opposite holds true for the V_3 correlations, the values being $+\frac{1}{3}$ and $-\frac{1}{3}$ for pyrolusite and ramsdellite, respectively. All low-energy structures have a nearest-neighbor correlation (V_1) that is –1, implying that always having vacancies stack on top of Mn along the c-axis is a requirement for low energy. The c-axis ordering makes sense since the nearest-neighbor sites along the c-axis share an octahedral face and are only ≈ 2.40 Å apart for most of the MnO_2 polymorphs.

For those structures that always have perfect –1 correlation along the c-axis, the 3D interaction model can be renormalized to a 2D one (since the configuration of Mn and vacancies in one plane fully characterizes the

configuration in any other plane, every 3D interaction can be reduced to a corresponding 2D interaction within the hexagonal plane). The renormalized interactions are shown in Fig. 9. To limit confusion we have kept the same numbering scheme as in the 3D model. Hence, the interactions listed as "2NN" is the first-neighbor interaction in a hexagonal plane.

Fig. 9 reveals the source of much of the near structural degeneracy in MnO_2. While the 3D interactions are strong, the renormalized effective 2D interactions are very small and frustrated. Hence, almost any configuration of Mn in the 2D plane, which preserves perfect *c*-axis correlation, will be low in energy. Clearly, this is the case for the low-energy configurations in Table 1. The model presented by Chabre and Pannetier [2] is essentially this 2D renormalized interaction model. We show below that while our model causes near structural degeneracy, it does not allow for thermal disorder at low temperature.

It may be noted that the paramagnetic energy correction (Table 3) has mainly positive ECI, making the total ECI slightly more repulsive (i.e. Mn–Mn repulsive or Mn–vacancy attractive) than for the purely ferromagnetic ECI. The fact that Mn ions repel each other slightly less in the ferromagnetic state than in the paramagnetic state (as parameterized by various AF arrangements) may be due to the fact that ferromagnetic spin order leads to more Mn–Mn electron hopping, and therefore reduces the electrostatic repulsion. Antiferromagnetism reduces electron hopping as an electron has to pay the exchange penalty when going from an Mn ion with given spin to one with opposite spin. Hence, paramagnetic and antiferromagnetic spin states lead to higher repulsion among Mn ions. In this material, this effect changes the groundstate from ε'-MnO_2 (with a high number of in-plane nearest-neighbor Mn ions) to pyrolusite (with fewer in-plane Mn–Mn nearest neighbors).

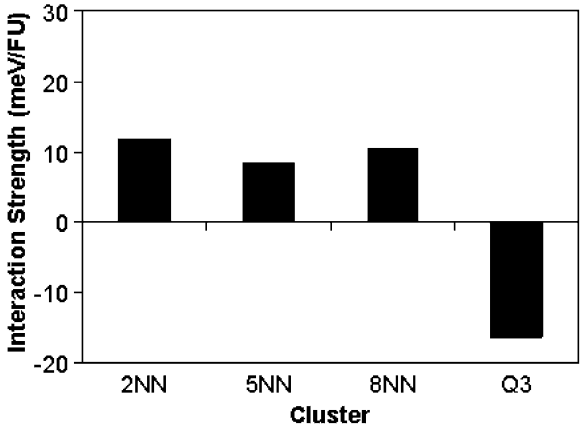

Fig. 9. The strength of the two-dimensionally renormalized ECIs in MnO_2. The relevant clusters are shown in Figs. 5 and 6.

4. Mn–vacancy thermodynamics

The finite temperature equilibration of the Mn–vacancy arrangement can be achieved using standard Monte Carlo equilibration of the Hamiltonian of Eq. (5) and with the total ECI from Table 3. Simulations were performed with a $10 \times 10 \times 10$ supercell of the primitive hexagonal cell (two lattice sites per cell) containing a total of 2000 lattice sites (consisting of 1000 Mn atoms and 1000 vacancy sites). The number of Monte Carlo steps per site was in the range 2500–3000 for each temperature and of those, the first 1000 were excluded from calculations of thermodynamic quantities to allow for equilibration. More details about Monte Carlo simulation can be found in Ref. [20].

4.1. Monte Carlo results

Fig. 10 shows the energy as function of temperature upon heating, clearly indicating a transition temperature from the ordered pyrolusite to a disordered state at about 3900 (K). Fig. 11(a–c) show snapshots of the structure at temperatures: 3000 (K) in (a), 3900 (K) in (b), and 4500 (K) in (c). Even though there are many structures with nearly the same energy, equilibrium Mn disorder only occurs at about 3900 (K). This apparent disparity can be explained by considering the 3D nature of the material: While the 2D model as proposed by Chabre and Pannetier [2] is useful to understand the possible structures that may form, it is misleading for understanding thermal excitations. Every Mn in the 2D model actually corresponds to a perfect column of alternating Mn vacancies along the *c*-axis. If we assume the *c*-axis correlation to be preserved, any perturbation of the 2D arrangement therefore corresponds to moving complete *c*-axis columns. Hence the energy for such an excitation will depend on the correlation length for ordering along the *c*-axis in the following way:

$$\Delta E_{\mathrm{exc}} \propto \xi_c \Delta e, \tag{6}$$

where Δe is the excitation energy in the 2D model and ξ_c is the correlation length along the *c*-axis. At low

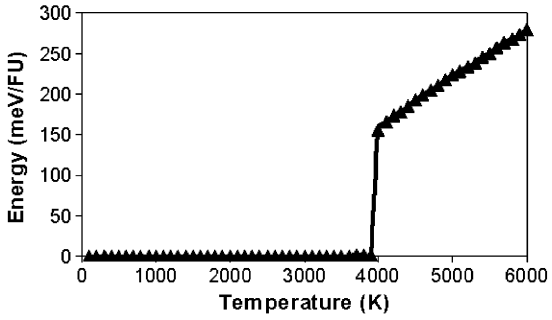

Fig. 10. Monte Carlo energy as a function of temperature for MnO_2.

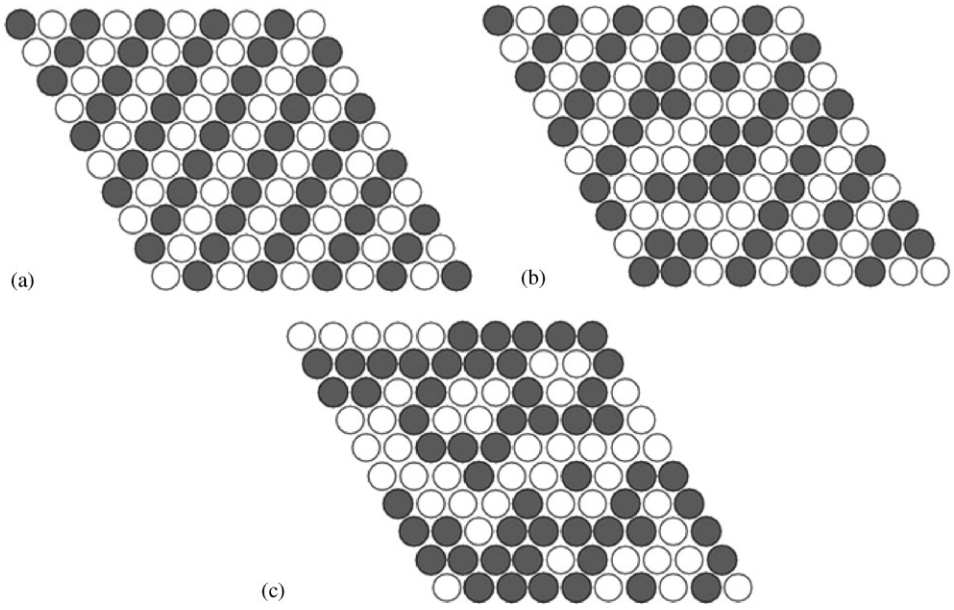

Fig. 11. Snapshot of the cationic lattice obtained from Monte Carlo simulations at $T = 3000$ (a), $T = 3900$ (b), and $T = 4500$ (c). Figure shows a basal plane of the hexagonal lattice. Dark and light circles represent Mn and vacancies, respectively.

temperature ξ_c approaches infinity and there are no low-energy excitations in the system. Only when ξ_c becomes of the order of 1 do the 2D excitations become available. Hence the order disorder temperature is largely determined by the *c*-axis correlation and the interaction in that direction. The strong V_1 interaction along the *c*-axis therefore sets the temperature scale for thermal disorder. A similar phenomenon exists in $YBa_2Cu_3O_x$ where chains of oxygen atoms and vacancies order. The oxygen atoms and vacancies have very small interactions between them but because of the length of the chains, the interaction *energy* between them is actually large [21]. The recent TEM and XRD observations by Bowden et al. [7] are consistent with these results. Even when disorder of Mn vacancies exists in one hexagonal plane, long-range correlation exists along the *c*-axis, making this effectively a disorder of 1D objects.

At room temperature, the theoretical equilibrium correlation length along the *c*-axis is likely to approach infinity. In a real material, the correlation length is limited by the grain size or the distance between defects. This brings up the possibility that the order/disorder temperature for Mn may be strongly influenced by the feature size of the MnO_2 crystals. In particular, in EMD, small domains or grains may limit the *c*-axis correlation length so that thermal disorder at relative low temperatures becomes possible.

Fig. 11(a) shows that pyrolusite is indeed the predicted ground state of the system at low temperatures. Only near the transition temperature (Fig. 11(b)) can thermal excitations be observed in this system. Hence, if the system were governed only by equilibrium thermodynamics, γ-MnO_2 should contain only pyrolusite and only at high temperatures, well above the decomposition temperature of real MnO_2, should disorder exists in the material. Therefore, the high disorder seen in real γ-MnO_2 at room temperature is *not due to equilibrium thermodynamic disorder of MnO_2*.

Defects could be a possible explanation for the structural complexity of γ-MnO_2 and hence calculations incorporating defects have been performed to study the effect of defects on the relative stability of various MnO_2 phases. The results, which are shown below, indicate that Ruetschi defects indeed introduce structural complexity in γ-MnO_2.

5. Effect of proton compensated Mn deficiencies

EMD generally contains about 4 weight percent of structural water in the crystal structure, which influences not only electrochemical reactivity but also other properties, such as density, electronic conductivity, and electrode potential [22–24]. Many studies have attempted to study the effect of structural water on the physical, chemical, and electrochemical properties of EMD [25,26]. At present, the cation vacancy model, proposed by Ruetschi [27], is the most successful model for explaining EMD properties. According to this model, γ-MnO_2 contains Mn vacancies. Each vacancy is coordinated to, and electrostatically compensated by, four protons. The protons are present in the form of OH^- ions, which replace the O^{2-} ions in the lattice without significant changes in the lattice parameters. On the basis of this cation vacancy model, Ruetschi claimed that ramsdellite (R-MnO_2) is electrochemically much

more reactive than pyrolusite (β-MnO_2) because ramsdellite contains Mn vacancies and a corresponding water content that provides an initial starting concentration of protons, which are useful for proton transfer. In contrast, pyrolusite contains almost no vacancies and thus very little water.

We have performed extensive first-principles calculations to show that Ruetschi defects have a profound effect on the relative stability of different MnO_2 polymorphs. The energies were determined using supercells, which force a certain ordering of the Ruetschi defects in the defected structure. No effort has been made to minimize the energy with respect to this ordering. In addition, although we fully relaxed the defects locally, it is easy for the four protons of the Ruetschi defect to get trapped in a local minimum. We attempted to find global minima, but some defects may have more stable arrangements than those which were located. These sources of error mean that the defect energies and arrangements given here must be viewed as qualitative, particularly in the more complex structures like twinned ramsdellite. Fig. 12 shows how the energy of different MnO_2 structures varies with the introduction of Ruetschi defects at varying concentrations. All energies are per Ruetschi defect and the results are given with respect to the Birnessite structure with 13% Ruetschi defects, for which the energy variation is set to zero. This fixes the reference energy of the Ruetschi defect (note that a Ruetschi defect concentration of X% means X% of the Mn have been replaced by Ruetschi defects). The influence of the Ruetschi defects is very significant, with their effect on the structure's energy varying over more than 0.8 eV. Since the important pure polymorphs tend to be within $\sim$100 meV of one another, a concentration of 5–10% Ruetschi defects can completely alter the relative stability of different polymorphs. Since real EMD can have Ruetschi defect concentrations of up to $\sim$8% [2] it is clear that Ruetschi defects must be considered in any analysis of MnO_2 structural stability. If Ruetschi defects are important for MnO_2 structural characteristics, one would expect there to be a correlation between Ruetschi defect concentration and structural changes. Such a correlation does seem to exist and is discussed at some length in Ref. [2].

Given the importance of Ruetschi defects, we have studied their energetics in more detail in order to understand what MnO_2 polymorphs they are likely to favor. Because Ruetschi defects contain four protons they can have many possible arrangements. It is this flexibility that allows the Ruetschi defect to interact so strongly with the Mn, since the defect can relax in response to different Mn arrangements. The most stable arrangement for Ruetschi protons in a Ruetschi defect are shown in Figs. 13–15, for pyrolusite, ramsdellite, and birnessite, respectively. After performing a large number of calculations we have extracted four simple conditions that guide the Ruetschi defect structure:

1. H attempt to bond covalently $\sim$1 Å from an O and Hydrogen bond $\sim$1.8 Å from another O.
2. H avoid Mn.
3. H avoid each other.
4. H stay near the defect site (the location of the missing Mn).

The Ruetschi defect is stable to the extent that it can satisfy all these conditions. For example, in birnessite, which consists of layers of filled and empty Mn sites, the Ruetschi defect is very unstable compared to other structures (see Fig. 12 for the energy and Fig. 15 for the

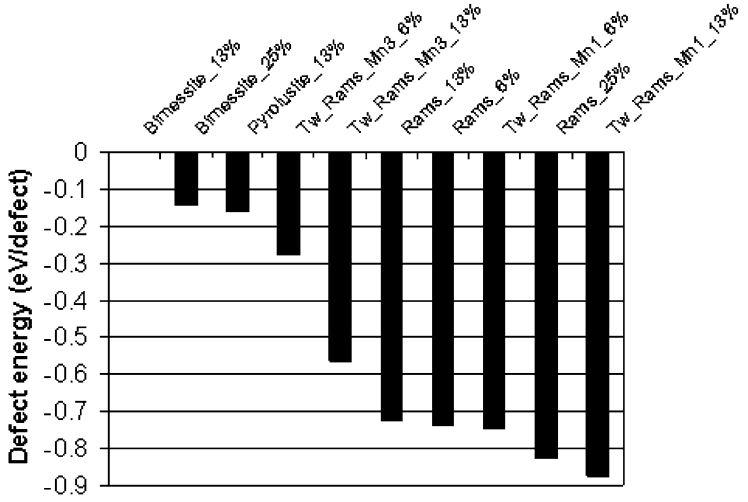

Fig. 12. Effect of Ruetschi defects on the structural energy for a number of different polymorphs and defect concentrations. "Rams" refers to ramsdellite and "Tw Rams" refers to fully twinned ramsdellite (see Fig. 2). Mn1 and Mn3 refer to two distinct sites in the twinned ramsdellite, with 3 and 5 nearest-neighbor Mn, respectively.

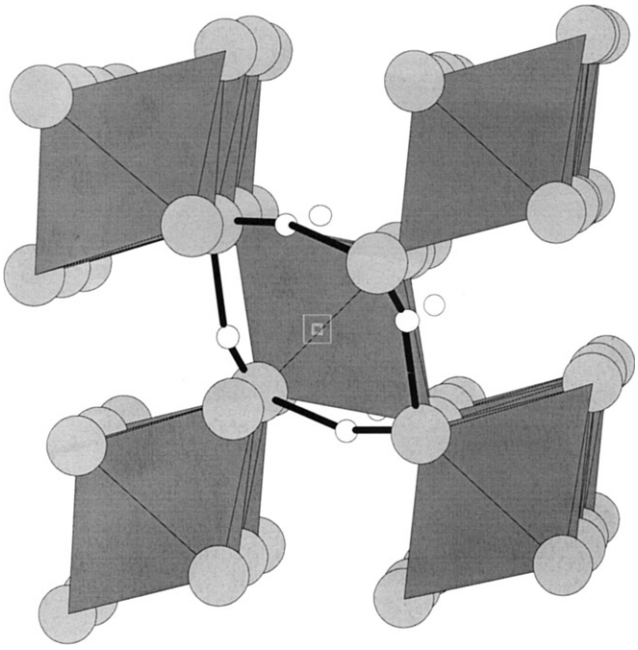

Fig. 13. Geometry of Ruetschi defects in pyrolusite. Oxygen are light gray circles. Mn octahedra are dark gray. H are small white circles and the covalent and hydrogen bonds with oxygen are shown as black lines. The absent Mn in the defect are represented by nested white squares.

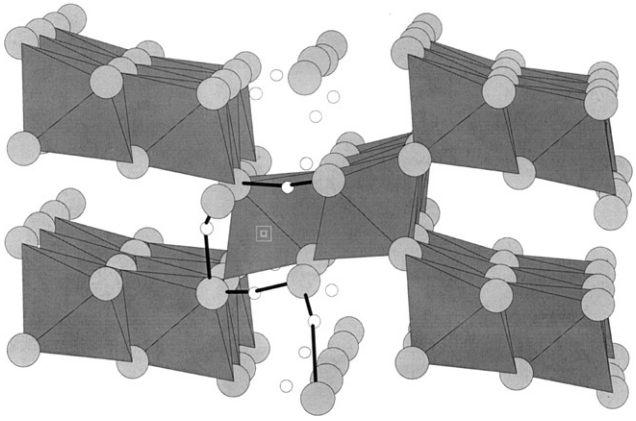

Fig. 14. Geometry of Ruetschi defects in ramsdellite. Oxygen are light gray circles. Mn octahedra are dark gray. H are small white circles and the covalent and hydrogen bonds with oxygen are shown as black lines. The absent Mn in the defect are represented by nested white squares.

fully relaxed Ruetschi defect structure). The compensating protons cannot enter the plane of the Mn because of condition 2, and cannot sit in the plane of the vacancies because of 1 (the oxygen planes separated by the vacancy layer are very far apart and a hydrogen cannot form both covalent and H-bonds while in the vacancy plane). This causes the protons to pack together near the defect and rather close to each other, violating condition 3 and causing the energy to go up. Ruetschi defects are also relatively unstable in pyrolusite, since it has only

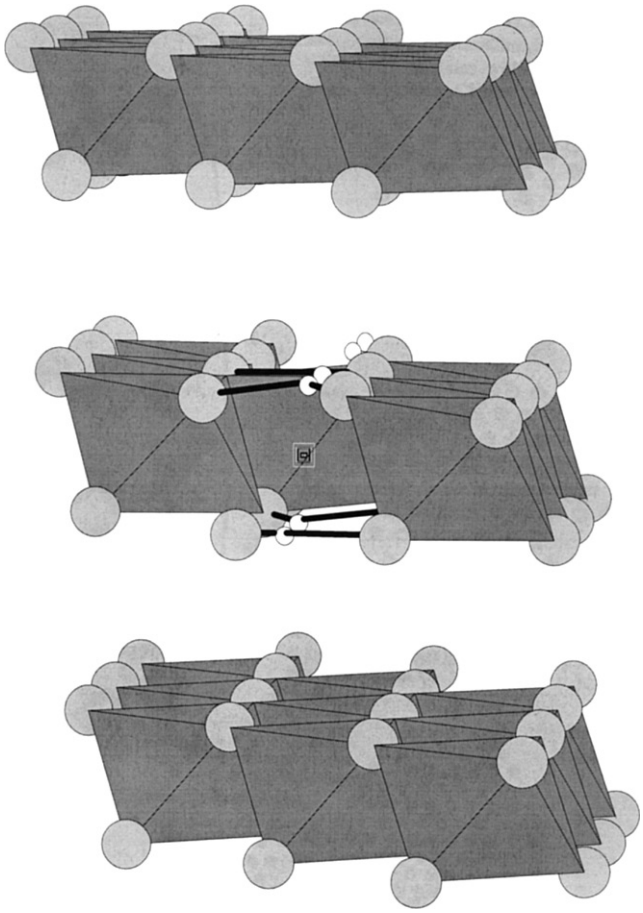

Fig. 15. Geometry of Ruetschi defects in birnessite. Oxygen are light gray circles. Mn octahedra are dark gray. H are small white circles and the covalent and hydrogen bonds with oxygen are shown as black lines. The absent Mn in the defect are represented by nested white squares.

1×1 tunnels and the protons cannot get very far from the Mn (see Fig. 12 for the energy and Fig. 13 for the fully relaxed Ruetschi defect structure). The ramsdellite structure is a better environment for Ruetschi defects since the 2×1 tunnels allow the Ruetschi protons to satisfy all the conditions at once without getting too close to a Mn (see Fig. 12 for the energy and Fig. 14 for the fully relaxed Ruetschi defect structure).

The four conditions tend to favor stable Ruetschi defects in "open" structures. These are structures where there is open space, far from the Mn, in which the Ruetschi protons can form low-energy arrangements with the oxygen. The increase in Ruetschi defect stabilization for more open structures can be seen in Fig. 12, where the less open birnessite and pyrolusite offer the lowest stabilization of the Ruetschi defects. What makes a structure open are attributes such as the large 2×1 tunnels in ramsdellite. Birnessite might seem a very open structure but the distance between the oxygen planes around the vacancies is too large to be useful to the Ruetschi protons.

In conclusion, it has been shown that the complex structure of the Ruetschi defects makes their stability couple very strongly to Mn arrangements. This coupling will drive the formation of more open MnO_2 polymorphs in highly defected materials. By altering the MnO_2 structure, Ruetschi defects have an indirect effect on cathode voltage and performance. Although we have not discussed it here, Ruetschi defects will also interact directly with intercalated hydrogen. The effect of these interactions on cathode voltage are discussed in Ref. [28].

6. Summary

Both synthetic and natural MnO_2 appear in a large number of polymorphs. Our first-principles calculations confirm that even though the effective Mn–Mn interactions are very large and repulsive, a number of structures are nearly degenerate in energy with pyrolusite. These structures can often be seen as different compromises to the frustration of the $V_1-V_2-V_3$ triangle of repulsive interactions. While pyrolusite prefers to maximize its in-plane nearest-neighbor Mn–vacancy pairs, ramsdellite sacrifices these to maximize its out-of-plane Mn–vacancy pairs. It is worth pointing out that since the in-plane and out-of-plane pairs are along different crystallographic axes, small changes in these parameters, as for example may occur with stress or defects, could modify the energy balance between ramsdellite and pyrolusite.

All low-energy structures have the lines of face-sharing octahedra along the *c*-axis occupied alternately by Mn atoms and vacancies. This can be rationalized by the short distance between these octahedral sites, which prevents their simultaneous occupation by Mn. This strong correlation along the *c*-axis transforms the disorder problem into one of organizing long Mn–vacancy–Mn chains. This can be turned into a 2D model by specifying the ion in the chain that penetrates a given plane perpendicular to the chain. The effective interactions between these chains, and per unit length of the chain, are very small, about 10–20 meV, which may be a cause of the structural diversity of MnO_2.

Our calculations also reconfirm the important role of magnetism in the energetics of manganese oxides [11]. Only when paramagnetic results are extrapolated from a large number of ferromagnetic and antiferromagnetic configurations does pyrolusite appear as the ground state of MnO_2, in agreement with the general interpretation of experimental results.

We have established that no thermal disorder exists in room temperature stoichiometric MnO_2, as permutations of the Mn–vacancy–Mn chains have a high-energy cost. Only when the correlation length is reduced can the system disorder. These ideas have been confirmed by direct Monte Carlo simulation on a lattice model derived from the density functional theory calculations.

The effect of Ruetschi defects, Mn vacancies compensated by four protons, is striking. We find that the coupling between Ruetschi defects and Mn ordering is so strong that one cannot consider the latter without including the effects of the former. Based on a number of calculations, we propose four guidelines for understanding Ruetschi defect stability. These rules follow from the tendencies for H to form covalent and hydrogen bonds to O, as well as basic electrostatic repulsion and charge compensation. The rules suggest that Ruetschi defects will help stabilize more open Mn arrangements than pyrolusite. As a specific example, even at low concentration, we predict that Ruetschi defects stabilize ramsdellite as compared to pyrolusite. This may explain the abundance of ramsdellite in Electrochemical MnO_2 (EMD), which is known to contain a substantial number of Ruetschi defects [19]. Our result that the energy of ramsdellite is lowered compared to pyrolusite is in agreement with the experimental observation [29] that Ruetschi defects predominantly occur in ramsdellite. The statement that Ruetschi defects are lower in energy in ramsdellite than in pyrolusite is formally equivalent to our finding that they stabilize ramsdellite over pyrolusite. Our results suggest that a possible way to control the relative amounts of ramsdellite and pyrolusite in γ-MnO_2 is to control the defect content.

In any γ-MnO_2 sample, the concentration of Ruetschi defects may be substantially higher in the ramsdellite units of γ-MnO_2 than the sample average, as the energy for the defect is lowest in ramsdellite and hence Ruetschi defects may segregate there. The transformation of ramsdellite into pyrolusite [30] upon heating could be explained by the loss of structural water, which reduces the Ruetschi defect concentration and hence the stability of ramsdellite.

It is not yet understood how the structural effects of Ruetschi defects can be reconciled with the recent multiphase model proposed by Heuer et al. [3], though it is possible that Ruetschi defects, if mobile, could organize into more perfect structures. Further work to investigate this is underway.

7. Conclusions

- We present one of the most extensive Density Functional Theory studies performed on the phase stability of a transition metal oxide, with over 300 calculations on various Mn and magnetic spin distributions on the octahedral sites of an hcp oxygen framework.
- Pyrolusite is the ground state of stoichiometric MnO_2 when paramagnetic Density Functional Theory

results are considered, which is in agreement with experiments. However, many structures that have perfect alternation of Mn atoms and vacancies along the *c*-axis have an energy very close to that of pyrolusite. Standard ferromagnetic spin polarization computations give incorrect results for the ground-state structure.

- Simulations suggest that thermal disorder is not the reason for the structural complexity in γ-MnO_2. If the system is governed by only thermodynamics, stoichiometric MnO_2 should contain only pyrolusite at room temperature. Several thousand degrees are needed to induce thermal disorder in stoichiometric pyrolusite MnO_2.
- Ruetschi defects could be the reason for the structural complexity of γ-MnO_2. Ruetschi defects stabilize ramsdellite and twinning over pyrolusite and introduce disorder in the material.

Acknowledgments

This work was performed with the support of Energizer Battery Corporation. The authors gratefully acknowledge discussions held with Dr. Paula Hughes, Dr. Huang Weiwei, Dr. Aron Newman, Dr. Scott Donne, Mr. Alan Ayers, Dr. Frank Feddrix, and Professor Art Heuer.

References

[1] O. Schilling, J.R. Dahn, J. Appl. Crystallogr. 31 (pt.3) (1998) 396.
[2] Y. Chabre, J. Pannetier, Prog. Solid State Chem. 23 (1995) 1.
[3] A.H. Heuer, A.Q. He, P.J. Hughes, F.H. Feddrix, in: IBA-2000 Manganese Oxide Symposium, Argonne National Laboratory, Chicago, IL, 2000.
[4] P.M. De Wolff, J.W. Visser, R. Giovanoli, R. Brütsch, Chimia 32 (1978) 257.
[5] P.M. De Wolff, Acta Crystallogr. 12 (1959) 341.
[6] D.E. Simon, T.N. Anderson, C.D. Elliott, in: IBA-2000 Manganese Oxide Symposium, Argonne National Laboratory, Chicago, IL, 2000.
[7] W. Bowden, R. Sirotina, S. Hackney, in: IBA-2000 Manganese Oxide Symposium, Argonne National Laboratory, Chicago, IL, 2000.
[8] A. Guinier, X-ray Diffraction, W.H. Freeman Company, San Francisco, 1963.
[9] M. Kaburagi, J. Kanamori, J. Phys. Soc. Jpn. 44 (1978) 718.
[10] G. Ceder, Comput. Mater. Sci. 1 (1993) 144.
[11] S.K. Mishra, G. Ceder, Phys. Rev. B 59 (1999) 6120.
[12] A. Van de Walle, G. Ceder, Rev. Mod. Phys. 74 (2001) 11.
[13] J.M. Sanchez, F. Ducastelle, D. Gratias, Physica A 128 (1984) 334.
[14] A. Van de Walle, G. Ceder, J. Phase Equilibria 23 (2002) 348.
[15] A. Van der Ven, M.K. Aydinol, G. Ceder, G. Kresse, J. Hafner, Phys. Rev. B 58 (1998) 2975.
[16] G. Kresse, J. Furthmüller, Comput. Mater. Sci. 6 (1996) 15.
[17] G. Kresse, J. Hafner, Phys. Rev. B 49 (1994) 14251.
[18] D. Morgan, B. Wang, A. van de Walle, G. Ceder, 2002, in press.
[19] W. Bowden, F. Wang, Y. Palk, C. Grey, in: IBA-2000 Manganese Oxide Symposium, Argonne National Laboratory, Chicago, IL, 2000.
[20] K. Binder, D.W. Heermann, Monte Carlo Simulation in Statistical Physics, Springer, Berlin, 1988.
[21] D. de Fontaine, G. Ceder, M. Asta, J. Less-Common Met. 164 (1990) 108.
[22] A. Kozawa, J. Electrochem. Soc. 106 (1959) 79.
[23] A.J. Brown, F.L. Tye, L.L. Wood, J. Electroanal. Chem. 122 (1981) 337.
[24] E. Preisler, J. Appl. Electrochem. 6 (1976) 311.
[25] P. Broulliet, A. Grund, F. Jolas, C. R. Acad. Sci. Paris 257 (1963) 3166.
[26] G. Coeffier, J. Brenet, Electrochim. Acta 10 (1965) 1013.
[27] P. Ruetschi, J. Electrochem. Soc. 131 (1984) 2737.
[28] D. Balachandran, D. Morgan, G. Ceder, J. Solid State Chem. 166 (2002) 463–476.
[29] P. Ruetschi, J. Electrochem. Soc. 135 (1988) 2657.
[30] R. Giovanoli, Thermochim Acta 234 (1994) 303.